

DIFFBLENDER: Scalable and Composable Multimodal Text-to-Image Diffusion Models

Sungnyun Kim^{1†} Junsoo Lee² Kibeom Hong^{3†} Daesik Kim² Namhyuk Ahn^{2‡}

¹KAIST AI ²NAVER WEBTOON AI ³Yonsei University

<https://sungnyun.github.io/diffblender/>

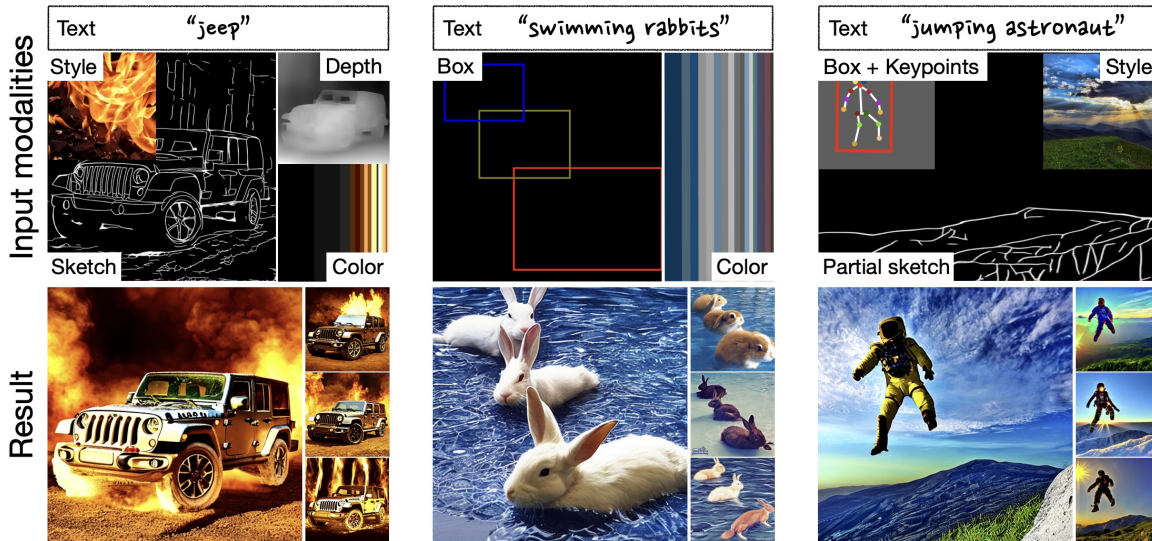


Figure 1. **Generated images with multimodal conditions.** By incorporating various types of input modalities (1st row), DIFFBLENDER successfully synthesizes high-fidelity and diverse samples, aligned with user preferences (2nd row).

Abstract

In this study, we aim to extend the capabilities of diffusion-based text-to-image (T2I) generation models by incorporating diverse modalities beyond textual description, such as sketch, box, color palette, and style embedding, within a single model. We thus design a multimodal T2I diffusion model, coined as DIFFBLENDER, by separating the channels of conditions into three types, i.e., image forms, spatial tokens, and non-spatial tokens. The unique architecture of DIFFBLENDER facilitates adding new input modalities, pioneering a scalable framework for conditional image generation. Notably, we achieve this without altering the parameters of the existing generative model, Stable Diffusion, only with updating partial components. Our study establishes new benchmarks in multimodal generation through quantitative and qualitative comparisons with existing conditional generation methods. We demonstrate that DIFFBLENDER faithfully blends all the provided information and showcase its various applications in the detailed image synthesis.

[†]Work done at NAVER WEBTOON AI; [‡]Corresponding author

1. Introduction

In the field of image generation, there has been a notable breakthrough due to the high generative capacity of text-to-image (T2I) generation models based on a diffusion process [9, 26, 43]. The observed growth can be attributed to the availability of extensive datasets containing pairs of images and corresponding text [20, 27, 40, 41], as well as aligning the image-text embedding space [29]. Latent Diffusion Models (LDM) [32] and its successor, Stable Diffusion (SD), have reduced computational cost of the diffusion process by executing diffusion at the latent level, also enabling a flexible text conditioning via cross-attention to the visual latents. Providing fine-grained descriptions solely through text prompts, however, can indeed limit utilization. Describing concrete details such as structural information (e.g., location, edge lines, and depth) or an abstract concept like the style of a reference image is not straightforward using text alone.

To address this challenge and enhance the image generation process, the incorporation of additional modalities alongside text has proven beneficial [11, 19, 24, 57, 60].

Nevertheless, these studies still have limitations: they are limited to supporting only one type of modality [19, 24, 57], involve training models with a substantial number of parameters [11, 57, 60], or support multimodal inference but require expensive cost for training independent networks [24].

Our goal is to propose an architectural design which can **1) compose diverse types of conditioning modalities within a single model**, and **2) provide an efficient and unified framework for scaling up the modalities**. To this end, we first categorize the input modalities into three types: image forms (*e.g.*, sketch and depth map), spatial (*e.g.*, object coordinates) and non-spatial (*e.g.*, color and style) token forms. Then, we establish our diffusion model, named **DIFFBLENDER**, which is composed of the conditioning modules for each modality type, attached to the SD backbone [32]. By updating only partial components while leaving the entire parameters of SD as itself, we not only retain its well-established knowledge but also ensure the model’s scalability of extending to additional input modalities.

Table 1 summarizes the technical difference with previous T2I diffusion models. Notably, DIFFBLENDER supports various modality types, provides multimodal training, and selectively updates partial components, which facilitates the scaling-up of supporting modalities. Figure 1 visualizes the generated samples of DIFFBLENDER, employing multiple conditions at once and successfully synthesizing the images as user preferences. Our contributions are listed as follows.

- We propose DIFFBLENDER to express complex combination of conditions, categorized into three distinct types.
- We design its structure to seamlessly extend to additional modalities without expensive training cost.
- The quantitative and qualitative evaluations verify the DIFFBLENDER’s multi-conditioning image synthesis.
- We introduce a novel guidance approach that allows delicate control of a specific modality, which is necessary for multimodal generation.

2. Related Work

Diffusion models. Diffusion models have gained significant attention as a promising approach for generating high-quality images [2, 9, 17, 25, 26, 30, 34–36, 38, 43]. They have shown superior performance compared to the adversarial models [5, 15, 39, 46, 52, 55] in terms of both fidelity and diversity [4]. Among them, LDM [32] proposed a unified and effective approach for conditional generation, being further developed into Stable Diffusion (SD). In this study, we leverage SD as a backbone diffusion model, enhancing our model’s wide applications.

Multimodal conditioning of T2I diffusion. Expressing fine-grained details (*e.g.*, spatial information) by text prompt is challenging. To alleviate this, several studies have expanded T2I diffusion models to incorporate additional conditioning modalities, such as sketches [48], depth

method	image forms	spatial tokens	non-spatial tokens	multimodal training	partial training
GLIGEN [19]	✗	✓	✗	✗	✓
T2I-Adapter [24]	✓	✗	✗	✗	✓
ControlNet [57]	✓	✗	✗	✗	▲
Uni-ControlNet [60]	✓	✗	✓	✓	▲
Composer [11]	✓	✗	✓	✓	✗
DIFFBLENDER	✓	✓	✓	✓	✓

Table 1. We summarize each T2I method’s supporting input modalities and training specifications—joint training of multiple modalities and the extent of updated components. ▲ of ControlNet and Uni-ControlNet indicates that its scale of learnable parameters is not full but more than half of the SD backbone [32].

maps [11, 57], boxes [45, 59], reference images [16, 56], scene graphs [13, 54], semantic maps [3, 18, 28, 50], or conjunction of concepts [21, 49].

Among them, Composer [11] is designed to condition on diverse modalities within a single model; however, it requires training the entire diffusion model from scratch, incurring significant training cost. ControlNet [57] and Uni-ControlNet [60] leverage the generative prior of SD [32] but still entail massive amount of data and time to update a large number of parameters, making it hard to scale up the modalities. In contrast, GLIGEN [19] and T2I-Adapter [24] address partial updates of conditioning modules, promoting efficient conditional image generation. However, these approaches are typically constrained to supporting only a single modality type [19, 24, 57], mostly image-based conditions. In this sense, we contribute to designing the SD-based networks that support a broader range of conditions, including image forms and spatial and non-spatial tokens, to enable extensive modality scaling and composition.

3. Method

3.1. Preliminaries on Latent Diffusion Models

To reduce the high computational cost of a diffusion process on the pixel space, LDM [32] learns a diffusion process on the latent space. A bi-directional mapping network is trained to produce the latent representation z of the image x , *i.e.*, $z = \text{enc}(x)$, $\tilde{x} = \text{dec}(z)$. Then, a UNet-based [33] denoising autoencoder is trained as a diffusion model on the latent z . Starting from the noise-induced z_T and conditioning on the image caption c , the diffusion model f_θ generates less noisy samples, gradually producing z_{T-1} to z_0 . The training objective of LDM is thus described as follows:

$$\min_{\theta} \mathcal{L}_{\text{LDM}} = \mathbb{E}_{z, \epsilon \sim \mathcal{N}(0, \mathbf{I}), t} [\|\epsilon - f_\theta(z_t, t, c)\|_2^2], \quad (1)$$

where t is uniformly sampled from time steps $\{1, \dots, T\}$, z_t is the step- t noisy latent of z , and $f_\theta(z_t, t, c)$ is the (t, c) -conditioned diffusion model. The denoising autoencoder is structured with several ResNet [7] and Transformer [47] blocks and predicts the noise $\hat{\epsilon}$ that has the same size as the input z . The time embedding is injected into each

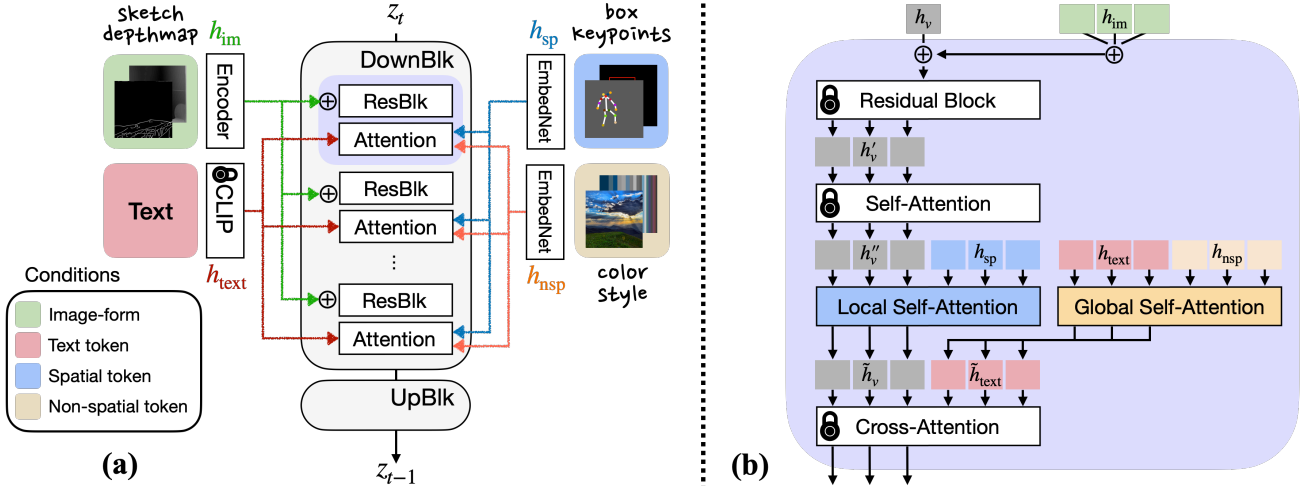


Figure 2. **Overview of DIFFBLENDER architecture.** (a) illustrates the four types of conditions including text employed in DIFFBLENDER and indicates where each part of information is used in the UNet layers. We note that spatial and non-spatial token conditions, although visually represented as images, are utilized as tokenized (or vectorized) forms. (b) focuses on the purple region in (a) to provide details of the DIFFBLENDER’s conditioning process. The lock-marked layers represent being fixed as the original parameters of SD [32]. The remaining parts, which are conditioning modules, indicate the learnable components of DIFFBLENDER.

ResNet block, as well as caption c conditioned via a cross-attention layer of Transformers. SD uses a pretrained CLIP encoder [29] to embed the caption into textual features before the cross-attention.

3.2. Architecture of DIFFBLENDER

We design DIFFBLENDER to ensure the model’s scalability, enabling the seamless integration and extension to a wide range of input modalities. To this end, we categorize modalities into three distinct types, each assigned to its specific conditioning module. The first type, referred to as image-form modality, contains spatially rich information such as sketches. Although this type of modality provides valuable conditioning data, it often requires extensive manual effort or the use of specialized processing tools.

To incorporate conditions that are more straightforward to use, such as box coordinates with grounding text or color choices from a palette, we design our model to additionally support tokenized representations. We employ two types of token-form conditions, namely spatial tokens and non-spatial tokens, as illustrated in Figure 2.

Latent fusion for image-form conditions. In order to incorporate image-form modalities, we have adopted sketches and depth maps. First, we obtain the latents $h_{im,k}$, for the k -th image-form modality, with an encoder network composed of small ResNet blocks [7]. Then, we fuse these latents with the original visual tokens h_v as an input to the residual block of the UNet: $h'_v \leftarrow \text{ResBlk}(h_v + \sum_k h_{im,k})$. Inspired by Mou *et al.* [24], we conduct this fusing step at four down-sampling ResNet blocks of the diffusion UNet [33] to ensure its effectiveness.

Besides, SD [32] consists of several self-attention (SA) and cross-attention (CA) layers in the Transformer blocks of UNet to combine the visual tokens and condition on the textual tokens. For convenience, this cross-attention is denoted as $CA(h''_v, h_{\text{text}})$, where $h''_v = SA(h'_v)$ are self-attended visual features, and h_{text} are textual features from the CLIP [29] encoder. DIFFBLENDER modifies the visual and textual features with spatial and non-spatial conditional tokens, respectively, which is described in the following.

Local self-attention for spatial tokens. To accurately locate the desired positions of synthesized results, we incorporate grounding box and keypoints as input modalities. Unlike textual information, spatial tokens have information that can directly affect visual tokens h_v to change the structure or semantics outputs. As result, users can assign where to place objects or how to pose a person in generated samples. To this end, we concatenate the self-attended visual tokens with all the spatial token conditions. Afterwards, we pass them through a local self-attention (LSA) module to obtain the intermediate visual tokens \tilde{h}_v (blue part in Figure 2 (b)).

$$\tilde{h}_v = h''_v + \text{LSA}([h''_v; \{h_{sp,i}\}]), \quad (2)$$

where $\text{LSA}(x) = \tanh(\beta_\ell) \cdot \text{SA}(x)[:V]$.

$h_{sp,i}$ are tokens for the i -th spatial condition, projected by our embedding network, and V is the visual token length. This LSA module is inspired by the gated attention mechanism in [1, 19] to gradually impose conditions on the intact visual tokens, gated with a learnable parameter β_ℓ .

Global self-attention for non-spatial tokens. In addition to the spatial modalities, DIFFBLENDER is also designed to

expropriate non-spatial conditions for guiding global expression. To this end, we set color palette and style embedding as non-spatial modalities. These contain global and abstract information that influences over the entire image, such as style, color, texture, brightness, etc. DIFFBLENDER concatenates non-spatial tokens with the original global information, textual tokens h_{text} . Subsequently, tokens are passed through a global self-attention (GSA) module to obtain the intermediate textual tokens \tilde{h}_{text} (yellow part in Figure 2 (b)).

$$\tilde{h}_{\text{text}} = h_{\text{text}} + \text{GSA}([\mathbf{h}_{\text{text}}; \{\mathbf{h}_{\text{ns},j}\}]), \quad (3)$$

where $\text{GSA}(\mathbf{x}) = \tanh(\beta_g) \cdot \text{SA}(\mathbf{x})[:L]$.

$h_{\text{ns},j}$ are tokens for the j -th non-spatial condition, and L is the textual token length. Consequently, the visual features are delivered to the next layer after cross-attending two intermediate features: $h_v \leftarrow \text{CA}(\tilde{h}_v, \tilde{h}_{\text{text}})$.

Training DIFFBLENDER. The training objective of DIFFBLENDER is similar to that of LDM [32]. DIFFBLENDER replaces c in Eq. 1 with $\mathbf{C} = \{c_{\text{text}}, c_{\text{sketch}}, c_{\text{box}}, \dots\}$ to leverage a set of modalities. It learns to denoise the latent z_t , given the time step t , with every condition in \mathbf{C} . For this, we prepare a set of image-caption pairs, extract every supporting conditions from the image (see Section 4.1), and input them to each conditioning module as described in Figure 2.

DIFFBLENDER allows for joint training of multiple modalities, although careful scheduling based on their properties may be needed. In our implementation, the sketches and depth maps provide detailed spatial information, which makes box or keypoints information redundant. This may impede the learning of modalities with less information but that are more user-friendly. We avoid this modality conflict by training spatial tokens first and image forms thereafter.

3.3. Mode-Specific Guidance for Controllability

Classifier-free guidance (CFG, [10]) is a simple yet effective method for conditional image generation [25, 37], modifying the predicted noise to include the gradient of the log-likelihood of $p(\mathbf{C}|\mathbf{x}_t)$. Given that $p(\mathbf{C}|\mathbf{x}_t) \propto p(\mathbf{x}_t|\mathbf{C})/p(\mathbf{x}_t)$, we can obtain $\nabla_{\mathbf{x}_t} \log p(\mathbf{C}|\mathbf{x}_t) \propto \epsilon^*(\mathbf{x}_t, \mathbf{C}) - \epsilon^*(\mathbf{x}_t)$ if we know their exact scores. Instead, $\nabla_{\mathbf{x}_t} p(\mathbf{x}_t|\mathbf{C})$ and $\nabla_{\mathbf{x}_t} p(\mathbf{x}_t)$ are parameterized via score estimators $\hat{\epsilon}(\mathbf{x}_t, \mathbf{C})$ and $\hat{\epsilon}(\mathbf{x}_t, \emptyset)$, conditional and unconditional noise estimators respectively, which are obtained by the denoising diffusion model. Thus, the adjusted noise prediction is $\hat{\epsilon}^*(\mathbf{x}_t, \mathbf{C}) = \hat{\epsilon}(\mathbf{x}_t, \emptyset) + w(\hat{\epsilon}(\mathbf{x}_t, \mathbf{C}) - \hat{\epsilon}(\mathbf{x}_t, \emptyset))$, where w is the guidance scale.

In our setup, where the condition set is multimodal, the CFG pushes every condition to the same level of guidance. Unlike unimodal generation, our multimodal generation requires more subtle modulation of input conditions. In order to guide a modality $c_m \in \mathbf{C}$ while other modalities are also given, we need to control the estimate of

$\nabla_{\mathbf{x}_t} \log p(c_m|\mathbf{x}_t, \mathbf{C} \setminus c_m)$, where

$$p(c_m|\mathbf{x}_t, \mathbf{C} \setminus c_m) = \frac{p(c_m, \mathbf{x}_t|\mathbf{C} \setminus c_m)}{p(\mathbf{x}_t|\mathbf{C} \setminus c_m)} \propto \frac{p(\mathbf{x}_t|\mathbf{C})}{p(\mathbf{x}_t|\mathbf{C} \setminus c_m)}.$$

Thus, the mode-specific guidance direction becomes $\hat{\epsilon}(\mathbf{x}_t, \mathbf{C}) - \hat{\epsilon}(\mathbf{x}_t, \mathbf{C} \setminus c_m)$, where the second term is obtained by using the null input for c_m while the other conditions are given. Consequently, the adjusted noise prediction for c_m , in addition to the original CFG, is

$$\hat{\epsilon}_m^*(\mathbf{x}_t, \mathbf{C}) = \hat{\epsilon}^*(\mathbf{x}_t, \mathbf{C}) + \gamma(\hat{\epsilon}(\mathbf{x}_t, \mathbf{C}) - \hat{\epsilon}(\mathbf{x}_t, \mathbf{C} \setminus c_m)),$$

where $\gamma \in \mathbb{R}$ is the controllable scale for mode-specific guidance. $\gamma < 0$ indicates reducing the impact of c_m , $\gamma > 0$ indicates increasing, and $\gamma = 0$ recovers the original CFG.

4. Experiments

4.1. Implementation Details

Preparing conditions. We train DIFFBLENDER on the widely-used benchmark, COCO2017 [20] train set, which contains nearly 120K real photos. For the conditional generation, we prepare the following input modalities: 1) *Sketch*: we utilize the PiDiNet [44] followed by a sketch simplification algorithm [42] to extract the sketch of an image. 2) *Depth map*: we employ the monocular depth estimation methods [31]. 3) *Grounding box / Keypoints*: we use the annotation data provided by COCO2017. Each box is tagged with a text that denotes the object class. 4) *Color palette*: to capture the color statistics of given images, we employ the smoothed CIELab histogram [14]. We set the CIELab palette space with 11 hue, 5 saturation, and 5 light values, and use a smoothing sigma of 10. 5) *Style embedding*: to embed style features from the given reference images, we employ the pretrained CLIP [29] image encoder.

Training. We train DIFFBLENDER with batch size 32 using $8 \times A100$ GPUs for 200K iterations; 150K iterations for training LSA and GSA with embedding networks, and the last 50K iterations for the image-form encoders. We set the learning rate as $5e-5$ for AdamW [22], with the first 10K warm-up iterations. During the training, we apply the center crop to input images with a resolution of 512×512 . In addition, for the CFG [10], we randomly drop image-form conditions and others with 50% and 10% probabilities, respectively. We also use segmentation maps to randomly mask the fore-/background of the sketch, to enable robust training and conditioning on partial sketches. We provide details on the embedding networks for each modality in Appendix A.

Evaluation. For evaluation, we use 5K samples in the COCO2017 [20] validation set cropped to 512×512 resolution. The T2I models are typically evaluated with FID (Fréchet inception distance) [8] and CLIP score [29] to measure the fidelity of samples and the affinity with

method	train set (size)	inference modality	YOLO \uparrow	SSIM \uparrow	Depth \uparrow	FID \downarrow	CLIP \uparrow
GLIGEN [19]	COCO17 (120K)	Box	17.5	30.8	87.1	19.2	24.7
DIFFBLENDER (ours)	COCO17 (120K)	Box	15.8	30.8	87.2	19.6	25.0
ControlNet-softedge † [57]	Web (3M)	Sketch	19.6	38.0	88.7	18.0	24.9
T2I-Adapter-sketch [24]	COCO17 (120K)	Sketch	11.2	32.1	88.0	20.2	26.5
DIFFBLENDER (ours)	COCO17 (120K)	Sketch	12.3	33.5	87.9	16.7	25.6
ControlNet-depth † [57]	Web (3M)	Depth	16.9	34.9	88.8	19.3	24.5
T2I-Adapter-depth ‡ [24]	LAION-A (600K)	Depth	10.5	29.1	88.2	22.4	26.5
DIFFBLENDER (ours)	COCO17 (120K)	Depth	11.3	30.6	88.1	16.4	25.7
DIFFBLENDER (ours)	COCO17 (120K)	Sketch + Depth	14.1	33.0	88.3	16.9	24.5
DIFFBLENDER (ours)	COCO17 (120K)	All modalities	19.7	34.8	88.5	14.1	25.3

Table 2. **Evaluation on COCO17 validation set.** For DIFFBLENDER, the modalities unused during inference are provided as null inputs. GLIGEN and T2I-Adapter-sketch are both trained on COCO17 train set, same as DIFFBLENDER. On the contrary, † ControlNet-softedge/-depth are trained on a much larger dataset, 3M image-caption pairs from web, and ‡ T2I-Adapter-depth is trained on LAION-Aesthetics [40]. Note that ControlNet is based on SD ver.1.5 whereas the other models employ SD ver.1.4. We exclude Uni-ControlNet [60], a multimodal-trained version of ControlNet, due to its large train set size (10M) and poor FID performances (FID score >20).

their text descriptions. However, these metrics are insufficient to assess the model in multimodal settings. To this end, we also measure YOLO-v5 score [12] (AP $_{50}$) to evaluate the correspondence of generated images with the input bounding boxes, SSIM (structural similarity index) [51] with the extracted sketches, and Depth score calculated by $100 - (10 \times \ell_2\text{-distance with depth maps})$.

4.2. Comparison with Previous T2I Methods

To assess the multi-conditional generative capability, we perform a comparative study between DIFFBLENDER and the state-of-the-art T2I models that can involve non-textual conditions. During the inference, we extract all six modalities from each image in the validation set. DIFFBLENDER then generates an image based on these conditions. We also present inference results using a unimodal condition (other than text) to compare with the existing methods.

Quantitative evaluation. The quantitative evaluation results are summarized in Table 2. DIFFBLENDER with multimodal conditions can achieve not only high fidelity but also reliable capability of multi-conditional generation, exhibiting high scores in YOLO, SSIM, and Depth. Even with a unimodal condition, DIFFBLENDER remains competitive with previous approaches. We also highlight the FID gap between DIFFBLENDER with all six modalities (14.1) and with sketch + depth (16.9), implying that the incorporation of non-spatial modalities significantly enhances the generation quality. While ControlNet also achieves high conditional scores due to its large training dataset, it performs worse than DIFFBLENDER in FID and CLIP score.

Furthermore, employing the proposed mode-specific guidance enhances DIFFBLENDER’s conditional scores while maintaining low FID. For instance, stronger guidance on the box modality increases the YOLO score up to 20.1 with FID of 14.5, and sketch guidance increases SSIM up to 37.6 with FID of 15.8 (refer to Appendix B for details).

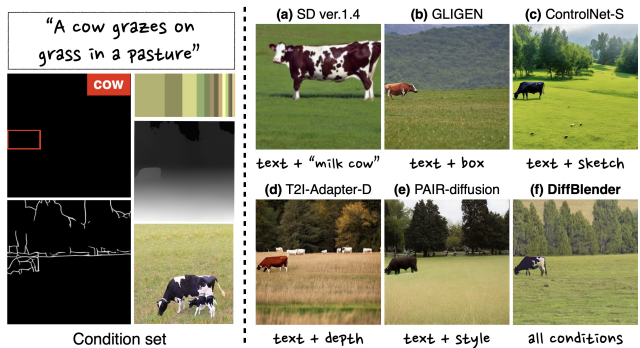


Figure 3. **Visual comparison with previous T2I methods.** Providing the conditions on the left, we present the comparative results generated by each model utilizing the available information. We set SD [32], GLIGEN [19], ControlNet-softedge [57], T2I-Adapter-depth [24], and PAIR-diffusion [6] as text-, box-, sketch-, depth-, and reference-based baselines over DIFFBLENDER, respectively.

DIFFBLENDER offers a broad range of conditioning options, whereas GLIGEN, ControlNet, and T2I-Adapter are limited to a single type of spatial modalities. They require users to convert their modalities into the type which it supports, such as patch shuffling of an image to mimic the color condition. Besides, there have been recent efforts to combine independently trained networks for multimodal inference, *e.g.*, CoAdapter or multi-ControlNet, but they require millions of images for training a certain modality. In contrast, we use only 120K images to train six modalities at once.

Qualitative evaluation. Figure 3 provides a visual comparison, where the samples are generated using the available condition(s) for each model. GLIGEN can guide the object’s position to some extent compared to SD, however, it does not reflect finer details. ControlNet and T2I-Adapter can spatially incorporate object details by leveraging the sketch or depth map but has intrinsic limitation in capturing the global style. PAIR-diffusion can condition on the reference

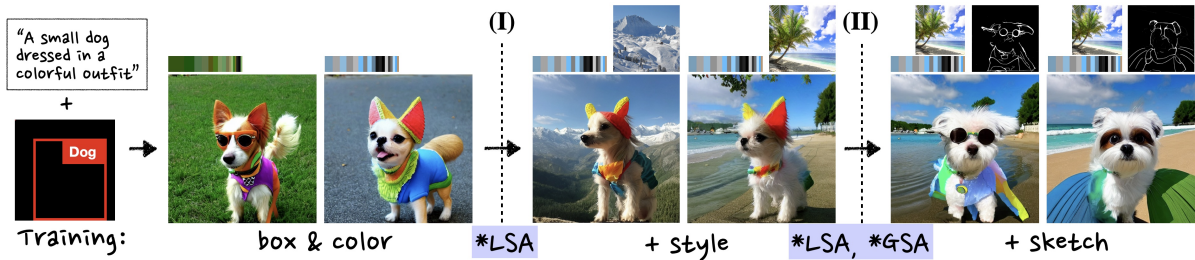


Figure 4. **Simulation of extending input modalities.** Once we finish training LSA and GSA with box and color conditions, (I) we then train the GSA module with style embedding while freezing (*) LSA. (II) Subsequently, we freeze both the LSA and GSA modules, followed by training the image-form encoder network for the sketch condition.

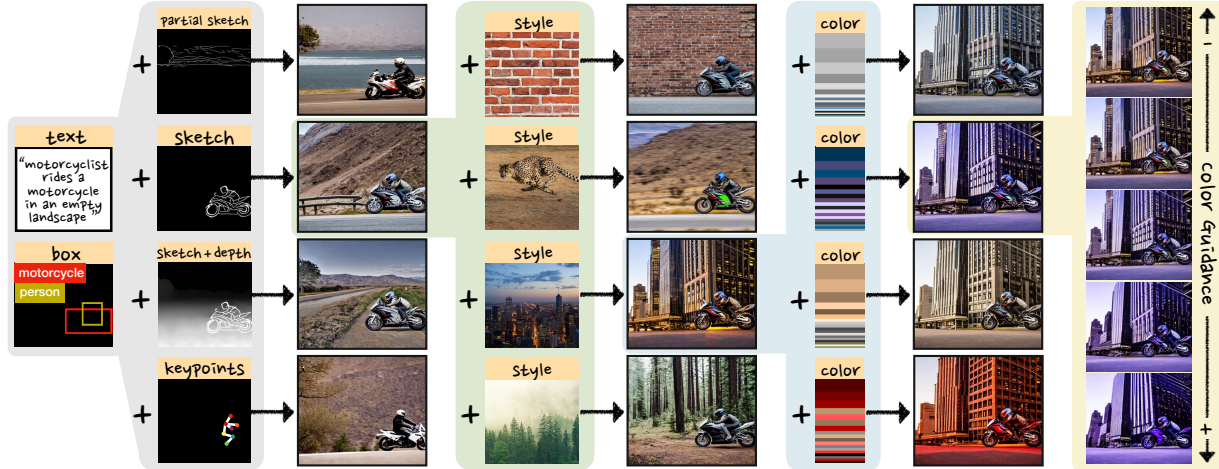


Figure 5. **Versatile applications of DIFFBLENDER.** DIFFBLENDER enables flexible manipulation of conditions, providing the image generation aligned with user preferences. Note that all results are generated by our single model at once, not in a sequence.

image, but its usage is bounded because it requires input pair images sharing identical semantic objects. In contrast, DIFFBLENDER has the advantage of utilizing various conditions within a single model, and we can specify not only the layout but also detailed poses or reference image information.

Human evaluation. To clearly evaluate the faithfulness of color or style conditioning, we have conducted a human perception test through user studies (see Appendix C for the questionnaire). In the A/B test, 81.9% of respondents indicated that the images from DIFFBLENDER matched the provided colors better, compared to the unconditionally generated images. Furthermore, the majority of users (88.6%) found the images generated by DIFFBLENDER more faithfully reflected the reference images than those from PAIR-diffusion [6]. Notably, 65.7% of users felt that DIFFBLENDER best followed their generative intention over the T2I baselines, thanks to its multi-conditioning ability.

Scalability by modality extension. Ideally, a multimodal T2I model should seamlessly adapt to new modalities without requiring any change to the underlying structure. However, previous works focusing on multimodal training [11, 60] have not addressed the modality extension task, due

to the substantial number of parameters to be trained and the inherent challenge of accommodating new modalities within their proposed architectural design. On the other hand, DIFFBLENDER is comprised of three modules according to the modality type and has a flexible mechanism to fuse more image-form conditions or concatenate more tokens.

To validate the scalability and adaptability of DIFFBLENDER, we simulate the modality extension scenario. As observed in Figure 4, new modalities can be simply supported with minimal computational cost while the previously learned conditioning information being also preserved. The scalability of DIFFBLENDER makes it easy to incorporate new modalities on demand. By training only partial components rather than re-training the entire model, users can extend the model to accumulate their own input modalities, further enhancing its performance and applicability.

4.3. Qualitative Results of DIFFBLENDER

Multimodal-conditioned generation. DIFFBLENDER exhibits the ability to generate images by incorporating various types of conditions and can even imagine missing modalities if they are not explicitly provided (Figure 1). DIFFBLENDER also opens up possibilities for numerous application scenar-

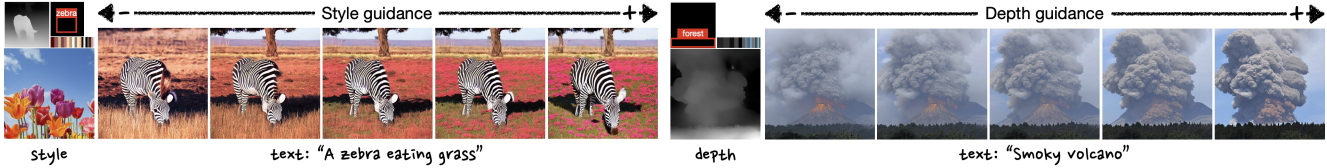


Figure 6. **Mode-specific guidance.** We linearly change the mode-specific guidance scale γ , where the center indicates $\gamma=0$ (original CFG).

ios, as depicted in Figure 5, where we have showcased a series of scenarios—starting with text and boxes, utilizing image-forms to specify the background layout or specify the human’s detailed posture, providing reference images for the abstract style, allowing free combination of colors, and even adjusting the strength of condition by controlling the mode-specific guidance.

Controlling mode-specific guidance. When conditioning a combination of diverse input modalities, it may be difficult for the model to impose every modality at the same level. We thus designed the way to guide a specific modality, formally described in Section 3.3. In Figure 6, we present two examples of mode-specific guidance, on the style embedding and depth map. The style guidance in a positive direction, strengthened by the reference image, draws flowers on the grass, whereas negative guidance removes them. Also, if we desire to increase the effect of the depth map to emphasize the smoke of a volcano, we can increase its guidance as presented. Note that while the mode-specific guidance enhances controllability, information from other modalities like box or color is still being preserved.

The CFG scale [10], w , is conventionally set as [5.0, 20.0], empirically found in the literature [32]. Because our mode-specific guidance is added to the original CFG, we set γ no less than $-w$ value; otherwise, it will not only reduce the impact of modality but also degrade the image quality. Conversely, if we set γ too high, the image generation will highly depend on the specified modality. In our experiments, we use $w = 5.0$ and $\gamma \in [-3.0, 3.0]$.

Reference-guided and semantic-preserved generation. The preservation of an image’s underlying structure while altering its style is a practical challenge [16, 58]. DIFFBLENDER adeptly achieves this by extracting the sketch and depth map from a source structure image, as well as the style embedding and color palette from a reference image. Combining these conditions, DIFFBLENDER can synthesize images that blend the semantic and stylistic aspects. In Figure 7, DIFFBLENDER effectively conveys new style onto the source image while maintaining its structural information. Intriguingly, it can seamlessly combine two unrelated images, such as {jet, tiger} or {snowman, fire}.

Object reconfiguration. Thanks to the wide range of conditions available in DIFFBLENDER, it becomes possible to reconstruct scenes containing diverse objects. In Figure 8, we



Figure 7. **Reference-guided and semantic-preserved generation.** When a source image is provided, DIFFBLENDER demonstrates the results preserving the structure inherent in that image, while effectively incorporating the style elements from a reference image.



Figure 8. **Object reconfiguration.** DIFFBLENDER reconstructs a new scene from an input image by altering the object type or adapting to new grounding information.

extract a partial sketch of the background and the position of the object from the input image. By altering the prompt for each corresponding object, *e.g.*, *flowers* or *dollars*, it can reconfigure the output images by creatively filling in the empty regions. A notable difference between DIFFBLENDER’s object reconfiguration and traditional inpainting-based image editing [23, 35, 53] lies in the fact that our method can exactly locate the object in the scene, or include new grounding information like a *fork*.

4.4. Analysis

Manipulating token-form conditions. Unlike the image-form modalities that require human effort to craft the conditions, it is much easier to manipulate spatial or non-spatial token conditions due to their simplicity. In Figure 9 (a), (b), we manipulate the spatial condition to adjust the position or pose of an object. We observe the sun being located in different places and an astronaut’s arms being elevated. In Figure 9 (c), (d), we randomly select color palettes or reference images, interpolate between their latents, and apply them to generate samples. Remarkably, during the smooth transition across different colors, the seagulls’ positions are being preserved while the background composition under-

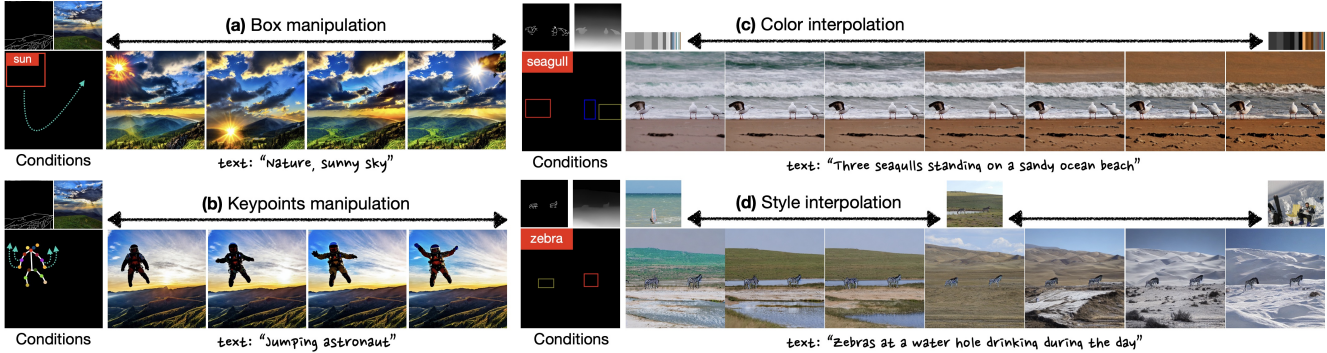


Figure 9. (a), (b): **Manipulation of the spatial conditions**, grounding box and keypoints. Throughout the shift, the partial sketch and reference image are consistently reflected. (c), (d): **Interpolation of the latent variables** of color palettes and reference image embeddings.

	0 – 150K	150K – 200K	YOLO \uparrow	FID \downarrow (box / all)
scheme A	I + S + N	I + S + N	13.1	18.9 / 14.8
scheme B	S + N	I + S + N	15.8	19.6 / 15.0
scheme C	S + N	I	15.6	18.7 / 14.1

Table 3. **Comparison between different training schemes of DIFFBLENDER**. For 200K iterations, training modality types are I (image forms), S (spatial tokens), and N (non-spatial tokens). YOLO score ($@AP_{50}$) is measured by conditioning only on the grounding box, while FID is measured on box / all six modalities.

goes imaginative changes. In the style interpolation case, substantial transformations are observed, especially in backgrounds, to actively incorporate the semantics and style of the reference image.

Training schemes. Table 3 shows the quantitative results of ablation study through the different training schemes of DIFFBLENDER. In scheme A, all modalities (I + S + N) are simultaneously trained over the entire span of 200K iterations. This model exhibits a subpar YOLO score (13.1), which implies that it has not properly learned the box modality. This suggests that the continuous provision of sketches and depth maps, both rich in spatial information, hinders the learning of box conditioning. To address this, we change the training scheme, where the image forms are only provided in the final 50K iterations, to avoid the modality conflict. We find that, in the second stage, training on the image forms alone (scheme C) makes the model with better FID scores than training altogether (scheme B). We thus adopt scheme C as our default training method.

Ablation study for non-spatial condition module. In the DIFFBLENDER’s design, we employ the GSA module to condition on the non-spatial token modalities by modifying the textual features. For ablation, we train the comparison model using only the LSA module, concatenating all the spatial and non-spatial tokens and self-attending them alongside with the visual features. Figure 10 displays that using LSA-only tends to prioritize color or style conditions over prompt details. For instance, the given color condition mistakenly



Figure 10. **Ablation experiment on the conditioning module for non-spatial tokens**, (a) using only LSA for every token-form condition, and (b) using LSA and GSA to segregate the channels of spatial and non-spatial conditions.

paints a red motorcycle blue. Conversely, introducing GSA delicately controls the generation because it regulates global information by only adjusting the textual features, compliant with the prompt. We highlight that it is important to analyze the characteristics of each modality and apply proper attention mechanisms for creating well-conditioned outputs.

5. Conclusion

We propose DIFFBLENDER, a novel multimodal T2I diffusion model that effectively incorporates diverse conditioning modalities and facilitates scaling up to additional input modalities. For this, we categorize the modality types into image forms, spatial tokens, and non-spatial tokens, and design the conditioning modules which can be efficiently trained. Through comprehensive evaluations with existing conditional generative models, our study establishes new benchmarks in the multimodal T2I generation. DIFFBLENDER demonstrates its impressive generation performance in faithfully blending complex combination of conditions, making it applicable to a wide range of use cases and enabling the mode-specific guidance to enhance controllability.

References

- [1] Jean-Baptiste Alayrac, Jeff Donahue, Pauline Luc, Antoine Miech, Iain Barr, Yana Hasson, Karel Lenc, Arthur Mensch, Katherine Millican, Malcolm Reynolds, et al. Flamingo: a visual language model for few-shot learning. *Advances in Neural Information Processing Systems*, 35:23716–23736, 2022. [3](#)
- [2] Huiwen Chang, Han Zhang, Jarred Barber, AJ Maschinot, Jose Lezama, Lu Jiang, Ming-Hsuan Yang, Kevin Murphy, William T Freeman, Michael Rubinstein, et al. Muse: Text-to-image generation via masked generative transformers. *arXiv preprint arXiv:2301.00704*, 2023. [2](#)
- [3] Guillaume Couairon, Jakob Verbeek, Holger Schwenk, and Matthieu Cord. Diffedit: Diffusion-based semantic image editing with mask guidance. *arXiv preprint arXiv:2210.11427*, 2022. [2](#)
- [4] Prafulla Dhariwal and Alexander Nichol. Diffusion models beat gans on image synthesis. *Advances in Neural Information Processing Systems*, 34:8780–8794, 2021. [2](#)
- [5] Patrick Esser, Robin Rombach, and Bjorn Ommer. Taming transformers for high-resolution image synthesis. In *Proceedings of the IEEE/CVF conference on computer vision and pattern recognition*, pages 12873–12883, 2021. [2](#)
- [6] Vidit Goel, Elia Peruzzo, Yifan Jiang, Dejia Xu, Nicu Sebe, Trevor Darrell, Zhangyang Wang, and Humphrey Shi. Pair-diffusion: Object-level image editing with structure-and-appearance paired diffusion models. *arXiv preprint arXiv:2303.17546*, 2023. [5](#), [6](#)
- [7] Kaiming He, Xiangyu Zhang, Shaoqing Ren, and Jian Sun. Deep residual learning for image recognition. In *Proceedings of the IEEE conference on computer vision and pattern recognition*, pages 770–778, 2016. [2](#), [3](#)
- [8] Martin Heusel, Hubert Ramsauer, Thomas Unterthiner, Bernhard Nessler, and Sepp Hochreiter. Gans trained by a two time-scale update rule converge to a local nash equilibrium. *Advances in Neural Information Processing Systems*, 30, 2017. [4](#)
- [9] Jonathan Ho, Ajay Jain, and Pieter Abbeel. Denoising diffusion probabilistic models. *Advances in Neural Information Processing Systems*, 33:6840–6851, 2020. [1](#), [2](#)
- [10] Jonathan Ho and Tim Salimans. Classifier-free diffusion guidance. *arXiv preprint arXiv:2207.12598*, 2022. [4](#), [7](#), [12](#)
- [11] Lianghua Huang, Di Chen, Yu Liu, Yujun Shen, Deli Zhao, and Jingren Zhou. Composer: Creative and controllable image synthesis with composable conditions. *arXiv preprint arXiv:2302.09778*, 2023. [1](#), [2](#), [6](#)
- [12] Glenn Jocher, Ayush Chaurasia, Alex Stoken, Jirka Borovec, Yonghye Kwon, Kalen Michael, Jiacong Fang, Zeng Yifu, Colin Wong, Diego Montes, et al. ultralytics/yolov5: v7. 0-yolov5 sota realtime instance segmentation. *Zenodo*, 2022. [5](#)
- [13] Justin Johnson, Agrim Gupta, and Li Fei-Fei. Image generation from scene graphs. In *Proceedings of the IEEE conference on computer vision and pattern recognition*, pages 1219–1228, 2018. [2](#)
- [14] Sergey Karayev. Rayleigh: search images by multiple colors. <https://github.com/sergeyk/rayleigh>, 2016. [4](#)
- [15] Tero Karras, Samuli Laine, and Timo Aila. A style-based generator architecture for generative adversarial networks. In *Proceedings of the IEEE/CVF conference on computer vision and pattern recognition*, pages 4401–4410, 2019. [2](#)
- [16] Gihyun Kwon and Jong Chul Ye. Diffusion-based image translation using disentangled style and content representation. *arXiv preprint arXiv:2209.15264*, 2022. [2](#), [7](#)
- [17] Wei Li, Xue Xu, Xinyan Xiao, Jiachen Liu, Hu Yang, Guohao Li, Zhanpeng Wang, Zhifan Feng, Qiaoqiao She, Yajuan Lyu, et al. Upainting: Unified text-to-image diffusion generation with cross-modal guidance. *arXiv preprint arXiv:2210.16031*, 2022. [2](#)
- [18] Yuheng Li, Yijun Li, Jingwan Lu, Eli Shechtman, Yong Jae Lee, and Krishna Kumar Singh. Collaging class-specific gans for semantic image synthesis. In *Proceedings of the IEEE/CVF International Conference on Computer Vision*, pages 14418–14427, 2021. [2](#)
- [19] Yuheng Li, Haotian Liu, Qingyang Wu, Fangzhou Mu, Jianwei Yang, Jianfeng Gao, Chunyuan Li, and Yong Jae Lee. Gligen: Open-set grounded text-to-image generation. In *Proceedings of the IEEE/CVF Conference on Computer Vision and Pattern Recognition*, pages 22511–22521, 2023. [1](#), [2](#), [3](#), [5](#), [12](#)
- [20] Tsung-Yi Lin, Michael Maire, Serge Belongie, James Hays, Pietro Perona, Deva Ramanan, Piotr Dollár, and C Lawrence Zitnick. Microsoft coco: Common objects in context. In *ECCV*, pages 740–755. Springer, 2014. [1](#), [4](#), [12](#)
- [21] Nan Liu, Shuang Li, Yilun Du, Antonio Torralba, and Joshua B Tenenbaum. Compositional visual generation with composable diffusion models. In *European Conference on Computer Vision*, pages 423–439. Springer, 2022. [2](#)
- [22] Ilya Loshchilov and Frank Hutter. Decoupled weight decay regularization. *arXiv preprint arXiv:1711.05101*, 2017. [4](#)
- [23] Andreas Lugmayr, Martin Danelljan, Andres Romero, Fisher Yu, Radu Timofte, and Luc Van Gool. Repaint: Inpainting using denoising diffusion probabilistic models. In *Proceedings of the IEEE/CVF Conference on Computer Vision and Pattern Recognition*, pages 11461–11471, 2022. [7](#)
- [24] Chong Mou, Xintao Wang, Liangbin Xie, Jian Zhang, Zhonggang Qi, Ying Shan, and Xiaoohu Qie. T2i-adapter: Learning adapters to dig out more controllable ability for text-to-image diffusion models. *arXiv preprint arXiv:2302.08453*, 2023. [1](#), [2](#), [3](#), [5](#), [13](#)
- [25] Alex Nichol, Prafulla Dhariwal, Aditya Ramesh, Pranav Shyam, Pamela Mishkin, Bob McGrew, Ilya Sutskever, and Mark Chen. Glide: Towards photorealistic image generation and editing with text-guided diffusion models. *arXiv preprint arXiv:2112.10741*, 2021. [2](#), [4](#)
- [26] Alexander Quinn Nichol and Prafulla Dhariwal. Improved denoising diffusion probabilistic models. In *International Conference on Machine Learning*, pages 8162–8171. PMLR, 2021. [1](#), [2](#)
- [27] Vicente Ordonez, Girish Kulkarni, and Tamara Berg. Im2text: Describing images using 1 million captioned photographs. *Advances in Neural Information Processing Systems*, 24, 2011. [1](#)
- [28] Taesung Park, Ming-Yu Liu, Ting-Chun Wang, and Jun-Yan Zhu. Semantic image synthesis with spatially-adaptive normalization. In *Proceedings of the IEEE/CVF conference on computer vision and pattern recognition*, pages 2337–2346,

2019. [2](#)
- [29] Alec Radford, Jong Wook Kim, Chris Hallacy, Aditya Ramesh, Gabriel Goh, Sandhini Agarwal, Girish Sastry, Amanda Askell, Pamela Mishkin, Jack Clark, et al. Learning transferable visual models from natural language supervision. In *International conference on machine learning*, pages 8748–8763. PMLR, 2021. [1](#), [3](#), [4](#), [12](#)
- [30] Aditya Ramesh, Prafulla Dhariwal, Alex Nichol, Casey Chu, and Mark Chen. Hierarchical text-conditional image generation with clip latents. *arXiv preprint arXiv:2204.06125*, 2022. [2](#)
- [31] René Ranftl, Katrin Lasinger, David Hafner, Konrad Schindler, and Vladlen Koltun. Towards robust monocular depth estimation: Mixing datasets for zero-shot cross-dataset transfer. *IEEE transactions on pattern analysis and machine intelligence*, 44(3):1623–1637, 2020. [4](#)
- [32] Robin Rombach, Andreas Blattmann, Dominik Lorenz, Patrick Esser, and Björn Ommer. High-resolution image synthesis with latent diffusion models. In *Proceedings of the IEEE/CVF Conference on Computer Vision and Pattern Recognition*, pages 10684–10695, 2022. [1](#), [2](#), [3](#), [4](#), [5](#), [7](#), [12](#), [18](#)
- [33] Olaf Ronneberger, Philipp Fischer, and Thomas Brox. U-net: Convolutional networks for biomedical image segmentation. In *Medical Image Computing and Computer-Assisted Intervention—MICCAI 2015: 18th International Conference, Munich, Germany, October 5–9, 2015, Proceedings, Part III 18*, pages 234–241. Springer, 2015. [2](#), [3](#)
- [34] Nataniel Ruiz, Yuanzhen Li, Varun Jampani, Yael Pritch, Michael Rubinstein, and Kfir Aberman. Dreambooth: Fine tuning text-to-image diffusion models for subject-driven generation. *arXiv preprint arXiv:2208.12242*, 2022. [2](#)
- [35] Chitwan Saharia, William Chan, Huiwen Chang, Chris Lee, Jonathan Ho, Tim Salimans, David Fleet, and Mohammad Norouzi. Palette: Image-to-image diffusion models. In *ACM SIGGRAPH 2022 Conference Proceedings*, pages 1–10, 2022. [7](#)
- [36] Chitwan Saharia, William Chan, Saurabh Saxena, Lala Li, Jay Whang, Emily L Denton, Kamyar Ghasemipour, Raphael Gontijo Lopes, Burcu Karagol Ayan, Tim Salimans, et al. Photorealistic text-to-image diffusion models with deep language understanding. *Advances in Neural Information Processing Systems*, 35:36479–36494, 2022. [2](#)
- [37] Chitwan Saharia, William Chan, Saurabh Saxena, Lala Li, Jay Whang, Emily L Denton, Kamyar Ghasemipour, Raphael Gontijo Lopes, Burcu Karagol Ayan, Tim Salimans, et al. Photorealistic text-to-image diffusion models with deep language understanding. *Advances in Neural Information Processing Systems*, 35:36479–36494, 2022. [4](#)
- [38] Chitwan Saharia, Jonathan Ho, William Chan, Tim Salimans, David J Fleet, and Mohammad Norouzi. Image super-resolution via iterative refinement. *IEEE Transactions on Pattern Analysis and Machine Intelligence*, 2022. [2](#)
- [39] Axel Sauer, Kashyap Chitta, Jens Müller, and Andreas Geiger. Projected gans converge faster. *Advances in Neural Information Processing Systems*, 34:17480–17492, 2021. [2](#)
- [40] Christoph Schuhmann, Romain Beaumont, Richard Vencu, Cade Gordon, Ross Wightman, Mehdi Cherti, Theo Coombes, Aarush Katta, Clayton Mullis, Mitchell Wortsman, et al. Laion-5b: An open large-scale dataset for training next generation image-text models. *arXiv preprint arXiv:2210.08402*, 2022. [1](#), [5](#)
- [41] Piyush Sharma, Nan Ding, Sebastian Goodman, and Radu Soricut. Conceptual captions: A cleaned, hypernymed, image alt-text dataset for automatic image captioning. In *Proceedings of the 56th Annual Meeting of the Association for Computational Linguistics (Volume 1: Long Papers)*, pages 2556–2565, 2018. [1](#)
- [42] Edgar Simo-Serra, Satoshi Iizuka, and Hiroshi Ishikawa. Mastering sketching: adversarial augmentation for structured prediction. *ACM Transactions on Graphics (TOG)*, 37(1):1–13, 2018. [4](#)
- [43] Jiaming Song, Chenlin Meng, and Stefano Ermon. Denoising diffusion implicit models. *arXiv preprint arXiv:2010.02502*, 2020. [1](#), [2](#)
- [44] Zhuo Su, Wenzhe Liu, Zitong Yu, Dewen Hu, Qing Liao, Qi Tian, Matti Pietikäinen, and Li Liu. Pixel difference networks for efficient edge detection. In *Proceedings of the IEEE/CVF international conference on computer vision*, pages 5117–5127, 2021. [4](#)
- [45] Wei Sun and Tianfu Wu. Image synthesis from reconfigurable layout and style. In *Proceedings of the IEEE/CVF International Conference on Computer Vision*, pages 10531–10540, 2019. [2](#)
- [46] Ming Tao, Hao Tang, Fei Wu, Xiao-Yuan Jing, Bing-Kun Bao, and Changsheng Xu. Df-gan: A simple and effective baseline for text-to-image synthesis. In *Proceedings of the IEEE/CVF Conference on Computer Vision and Pattern Recognition*, pages 16515–16525, 2022. [2](#)
- [47] Ashish Vaswani, Noam Shazeer, Niki Parmar, Jakob Uszkoreit, Llion Jones, Aidan N Gomez, Łukasz Kaiser, and Illia Polosukhin. Attention is all you need. *Advances in Neural Information Processing Systems*, 30, 2017. [2](#)
- [48] Andrey Voynov, Kfir Aberman, and Daniel Cohen-Or. Sketch-guided text-to-image diffusion models. *arXiv preprint arXiv:2211.13752*, 2022. [2](#)
- [49] Ruichen Wang, Zekang Chen, Chen Chen, Jian Ma, Haonan Lu, and Xiaodong Lin. Compositional text-to-image synthesis with attention map control of diffusion models. *arXiv preprint arXiv:2305.13921*, 2023. [2](#)
- [50] Tengfei Wang, Ting Zhang, Bo Zhang, Hao Ouyang, Dong Chen, Qifeng Chen, and Fang Wen. Pretraining is all you need for image-to-image translation. *arXiv preprint arXiv:2205.12952*, 2022. [2](#)
- [51] Zhou Wang, Alan C Bovik, Hamid R Sheikh, and Eero P Simoncelli. Image quality assessment: from error visibility to structural similarity. *IEEE transactions on image processing*, 13(4):600–612, 2004. [5](#)
- [52] Tao Xu, Pengchuan Zhang, Qiuyuan Huang, Han Zhang, Zhe Gan, Xiaolei Huang, and Xiaodong He. Attngan: Fine-grained text to image generation with attentional generative adversarial networks. In *Proceedings of the IEEE conference on computer vision and pattern recognition*, pages 1316–1324, 2018. [2](#)
- [53] Binxin Yang, Shuyang Gu, Bo Zhang, Ting Zhang, Xuejin Chen, Xiaoyan Sun, Dong Chen, and Fang Wen. Paint by example: Exemplar-based image editing with diffusion models. *arXiv preprint arXiv:2211.13227*, 2022. [7](#)

- [54] Ling Yang, Zhilin Huang, Yang Song, Shenda Hong, Guohao Li, Wentao Zhang, Bin Cui, Bernard Ghanem, and Ming-Hsuan Yang. Diffusion-based scene graph to image generation with masked contrastive pre-training. *arXiv preprint arXiv:2211.11138*, 2022. [2](#)
- [55] Hui Ye, Xiulong Yang, Martin Takac, Rajshekhar Sunderraman, and Shihao Ji. Improving text-to-image synthesis using contrastive learning. *arXiv preprint arXiv:2107.02423*, 2021. [2](#)
- [56] Xin Yuan, Zhe Lin, Jason Kuen, Jianming Zhang, and John Collomosse. Text-to-image generation via implicit visual guidance and hypernetwork. *arXiv preprint arXiv:2208.08493*, 2022. [2](#)
- [57] Lvmin Zhang, Anyi Rao, and Maneesh Agrawala. Adding conditional control to text-to-image diffusion models. In *Proceedings of the IEEE/CVF International Conference on Computer Vision*, pages 3836–3847, 2023. [1](#), [2](#), [5](#), [12](#), [13](#)
- [58] Yuxin Zhang, Nisha Huang, Fan Tang, Haibin Huang, Chongyang Ma, Weiming Dong, and Changsheng Xu. Inversion-based style transfer with diffusion models. In *Proceedings of the IEEE/CVF Conference on Computer Vision and Pattern Recognition*, pages 10146–10156, 2023. [7](#)
- [59] Bo Zhao, Lili Meng, Weidong Yin, and Leonid Sigal. Image generation from layout. In *Proceedings of the IEEE/CVF Conference on Computer Vision and Pattern Recognition*, pages 8584–8593, 2019. [2](#)
- [60] Shihao Zhao, Dongdong Chen, Yen-Chun Chen, Jianmin Bao, Shaozhe Hao, Lu Yuan, and Kwan-Yee K Wong. Uni-controlnet: All-in-one control to text-to-image diffusion models. *Advances in Neural Information Processing Systems*, 36, 2023. [1](#), [2](#), [5](#), [6](#)

DIFFBLENDER: Scalable and Composable Multimodal Text-to-Image Diffusion Models

Supplementary Material

A. Implementation Details

We provide a description of the embedding network architectures and address various hyperparameters that were not covered in detail within the main paper.

Embedding networks. In our implementation, we designed specific encoder networks for the sketch and depth map modalities. These encoder networks consist of 8 ResNet blocks, each containing 2 convolutional layers. To ensure compatibility with the original visual features in the UNet, downsampling layers are incorporated into the 3rd, 5th, and 7th ResNet blocks. Additionally, at the 2nd, 4th, 6th, and 8th blocks, the latents are output after passing through each zero-conv module [57], which gradually influences the latent fusion process. Prior to entering the encoder networks, each sketch or depth map is encoded using the autoencoder-KL [32], sharing the same encoder as the image. It is important to note that these pretrained autoencoders are frozen during our training pipeline.

Furthermore, we designed embedding networks for the remaining modalities. For grounding box and keypoints, we followed the annotation format of the COCO2017 dataset [20] and the implementation of GLIGEN [19]. Each image employs 30 bounding boxes and 8×17 keypoints (17 keypoints per person, 8 persons in total). Each bounding box has a text annotation, which is embedded using the CLIP text encoder [29], and 4-digit coordinates, which are embedded using Fourier embedding. These embeddings are concatenated and projected using a 3-layer MLP with a hidden dimension of 512 and an output dimension of 768. Similarly, each keypoint includes a person identification and 2-digit coordinates, which are embedded using person embedding and Fourier embedding, respectively. These embeddings are also concatenated and projected using a 3-layer MLP with a hidden dimension of 512 and an output dimension of 768.

As for the color palette and style embedding, both utilize an embedding network consisting of a 3-layer MLP with LayerNorm and SiLU activation layers. This MLP has a hidden dimension of 512 and an output dimension of 768. The style embedding is first embedded by the CLIP image encoder before being passed through the MLP, while the color palette histogram values are multiplied by 10 and then undergo Fourier embedding. We observed that this multiplication enables faster convergence due to the small magnitude of the histogram values.

Hyperparameters. During the training, we applied the transformations to the images, including random flipping and center cropping to a resolution of 512. To enable robust training and facilitate conditioning on partial sketches, segmentation maps are utilized to randomly mask the sketches. The probability of using the segmentation map is set to 0.7, and if used, the foreground or background of the sketch is masked with a probability of 0.5 for each. In terms of the classifier-free guidance [10], a drop ratio of 0.5 is employed for the image-form modalities, while a drop ratio of 0.1 is used for other modalities. Captions are dropped with a ratio of 0.1, and null inputs are utilized for the dropped modalities. For the null tokens within Transformer blocks, we used learnable null tokens initialized to zero, whereas non-trainable zero-filled tensors are used for null inputs of image-form conditions.

During the inference, two significant hyperparameters come into play: classifier-free guidance scale (w) and scheduling coefficient α . A classifier-free guidance scale of 5.0 is employed by default. α serves as scaling coefficients to schedule the conditioning strength during the inference. α_{im} is multiplied after the fusion of image-form latents, $\alpha_{\text{im}} \sum_k \mathbf{h}_{\text{im},k}$; α_{sp} is multiplied on the LSA module, $\alpha_{\text{sp}} \text{LSA}([\mathbf{h}_v''; \{\mathbf{h}_{\text{sp},i}\}])$; and α_{nsp} is multiplied on the GSA module, $\alpha_{\text{nsp}} \text{GSA}([\mathbf{h}_{\text{text}}; \{\mathbf{h}_{\text{nsp},j}\}])$. When T represents the total number of denoising diffusion steps, the values of α_{sp} and α_{nsp} are set to 1 for the first $0.3T$ steps, and then set to 0 for the remaining $0.7T$ steps. α_{im} remains at a constant value of 0.7 for all T steps. These hyperparameters were determined based on achieving the lowest FID score.

B. Quantitative Results of Mode-Specific Guidance

By adjusting the condition through mode-specific guidance, images are synthesized to reflect the specified condition more or less; however, excessive manipulation can result in a degradation in image quality. As detailed in the main paper, we shift the mode-specific guidance scale within the range of $[-3.0, 3.0]$ to preserve the image quality, while using a fixed value of 5.0 for the classifier-free guidance scale. Given the sensitivity of the image to sketch guidance, the guidance scale value for this modality is adjusted within the range of $[-1.5, 1.5]$.

Figure 11 presents quantitative results showing the effective control of mode-specific guidance, demonstrating the reliable control in terms of image quality and conditioning strength within a reasonable range of the guidance scale. We observe that YOLO score, SSIM, and Depth score all increase with an elevation of the guidance scale value. Conversely, reducing the scale value allows for decreasing the impact solely on the specified modality. Importantly, we note that mode-specific guidance has a minimal impact on FID scores, which remain significantly lower than those of other T2I methods (Table 2) such as GLIGEN (19.2), ControlNet (18.0), or T2I-Adapter (20.2).

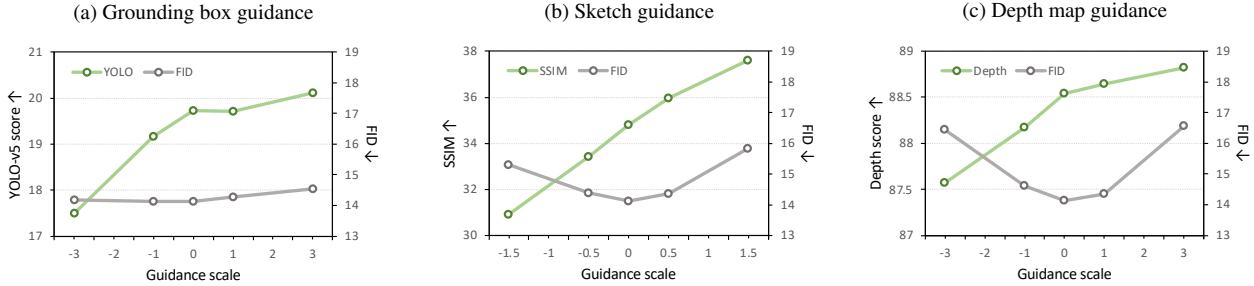


Figure 11. Quantitative evaluation of mode-specific guidance control, measured on COCO2017 validation set.

C. Human Evaluation

In addition to machine-based evaluation metrics such as YOLO score or SSIM, we conduct a user study to complement human perceptual assessment. Question 1 in Table 4 is designed to assess spatial condition faithfulness, revealing that DIFFBLENDER excels at customizing image generation according to user intentions (65.7%) due to its ability to condition on diverse modalities. Similarly, Questions 2 and 3 are designed to confirm the non-spatial condition faithfulness, on style embedding and color palette, respectively. DIFFBLENDER faithfully reflects the style of the reference image (88.6%) and accurately captures the color palette (81.9%). Lastly, Question 4 investigates the effectiveness of the mode-specific guidance in reliably controlling the specified modality while maintaining others.

Question	Result
[Question 1] Given the user’s intended image, which image most accurately reflects the user’s intention? [Options] Generated images from SD ver.1.4, ControlNet, GLIGEN, T2I-Adapter, and DIFFBLENDER.	SD ver.1.4 (0.0%), ControlNet (18.6%), GLIGEN (0.0%), T2I-Adapter (15.7%), DIFFBLENDER (65.7%)
[Question 2] Given the reference image, which image most accurately reflects the style of the reference image? [Options] Generated images from PAIR-diffusion and DIFFBLENDER.	PAIR-diffusion (11.4%), DIFFBLENDER (88.6%)
[Question 3] Given the color palette, which image most accurately reflects the provided colors? [Options] Generated images of DIFFBLENDER with or without the color palette condition.	with color conditioning (81.9%) without color conditioning (18.1%)
[Question 4] (1) Does mode-specific guidance change the output images? (2) Is the change reasonable according to the specified modality? (3) During the guidance, are the other modalities being maintained?	(1) Yes (96.8%), No (3.2%) (2) Yes (95.2%), No (4.8%) (3) Yes (97.6%), No (2.4%)

Table 4. **User study questionnaire and results.** In total, 42 respondents have participated. In **Question 1**, we provide the user with the originally intended image, extract every conditioning modality from the image, and generate conditional images with possible modalities for each model. For sketch conditions, we adopt ControlNet [57] as a softedge model and T2I-Adapter [24] as a sketch model, respectively, both open-sourced in the official code. For **Questions 1–3**, five examples and answers have been recorded per each question. For **Question 4**, three examples and answers have been recorded.

D. Additional Qualitative Results

We provide additional qualitative results of DIFFBLENDER, including mode-specific guidance, reference-guided generation, object reconfiguration, latent interpolation, and exploring failure cases.

D.1. Mode-Specific Guidance

Figure 12 presents the mode-specific guidance examples as in Figure 6, including sketch, depth, color, and style guidances.

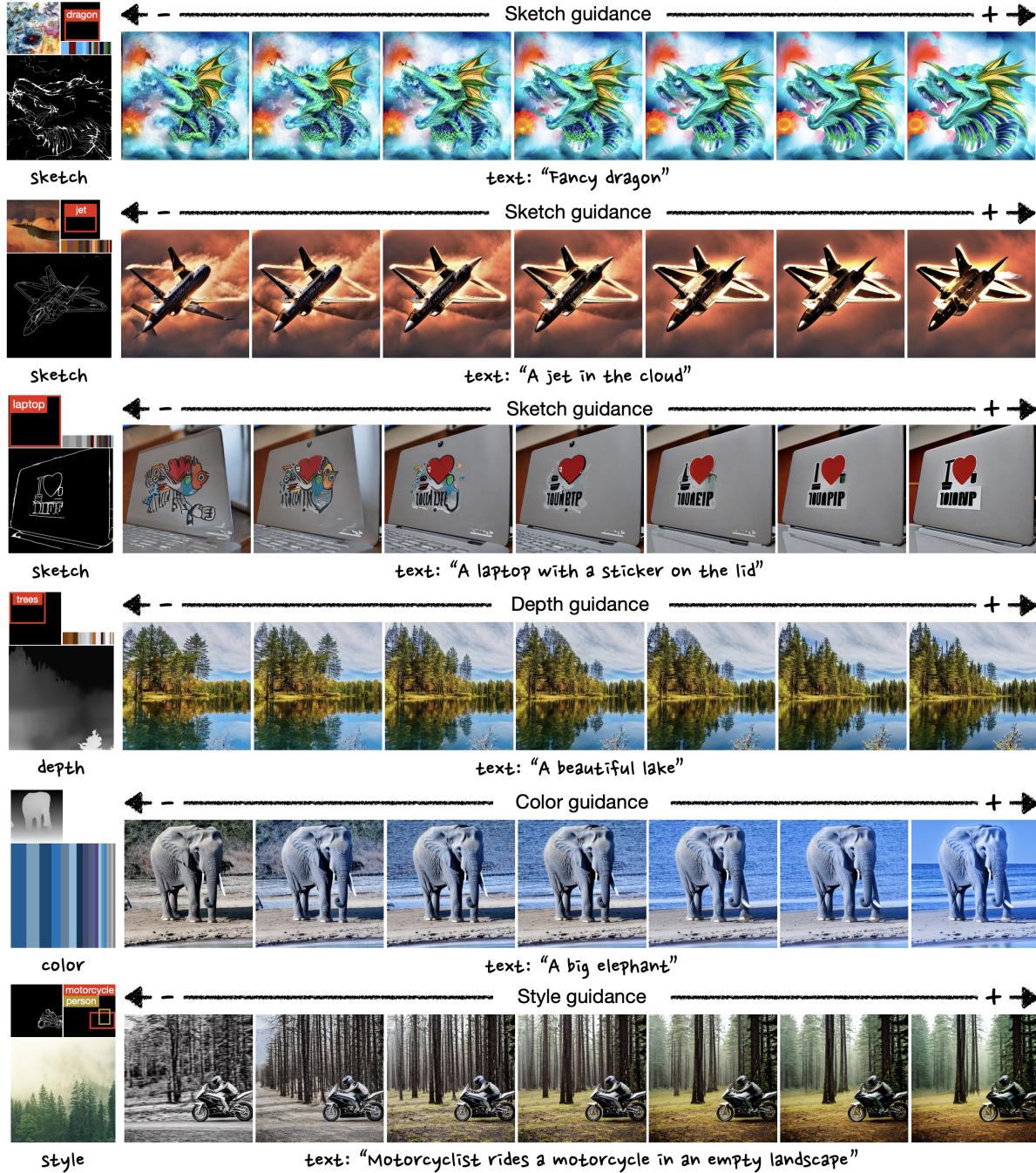


Figure 12. **Mode-specific guidance.** Each row depicts the mode-specific guided samples for each modality. We linearly change the scale γ , where the center indicates $\gamma = 0$ (original classifier-free guidance).

D.2. Reference-Guided Generation with Semantics

Figure 13 illustrates the reference-guided and semantic-preserved generation as in Figure 7.



Figure 13. **Reference-guided and semantic-preserved generation.** DIFFBLENDER effectively conveys the style from a reference image (top in the first column) while maintaining the structural information of a source image (bottom in the first column).

D.3. Object Reconfiguration

Figure 14 illustrates the object reconfiguration as in Figure 8, in this case with variations in the clothing.



Figure 14. **Object reconfiguration for clothes.** We extract a depth map of the violinist and specify the *clothes* region using a box. By altering the reference images associated with the clothing, it can reconfigure the scenes, modifying the outfit and style of the violinist.

D.4. Latent Interpolation

In addition to Figure 9, Figures 15 and 16 provide more examples on the latent interpolation of non-spatial conditions, color palette and style embedding, respectively.

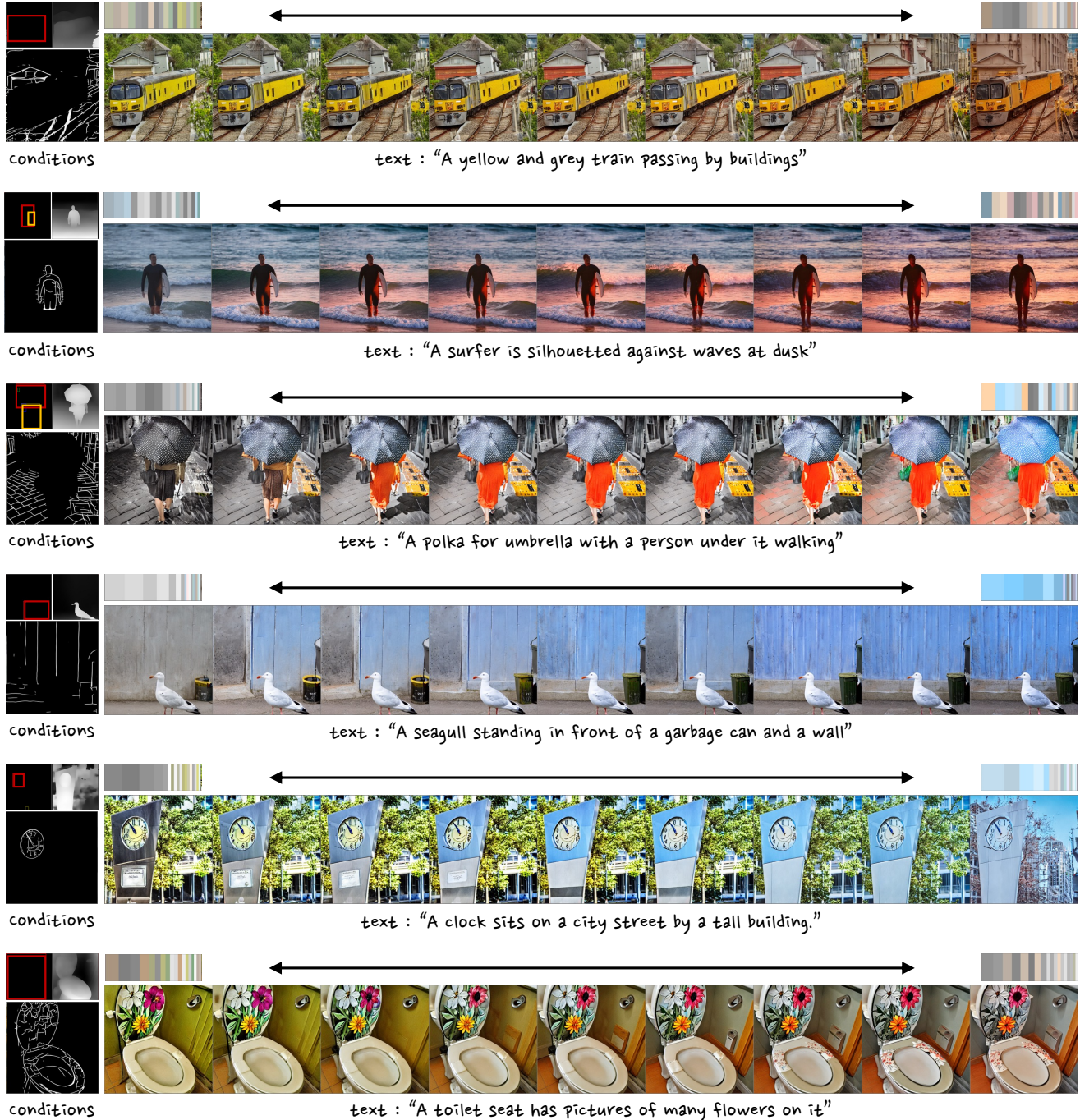


Figure 15. Interpolating latents for the color palette.

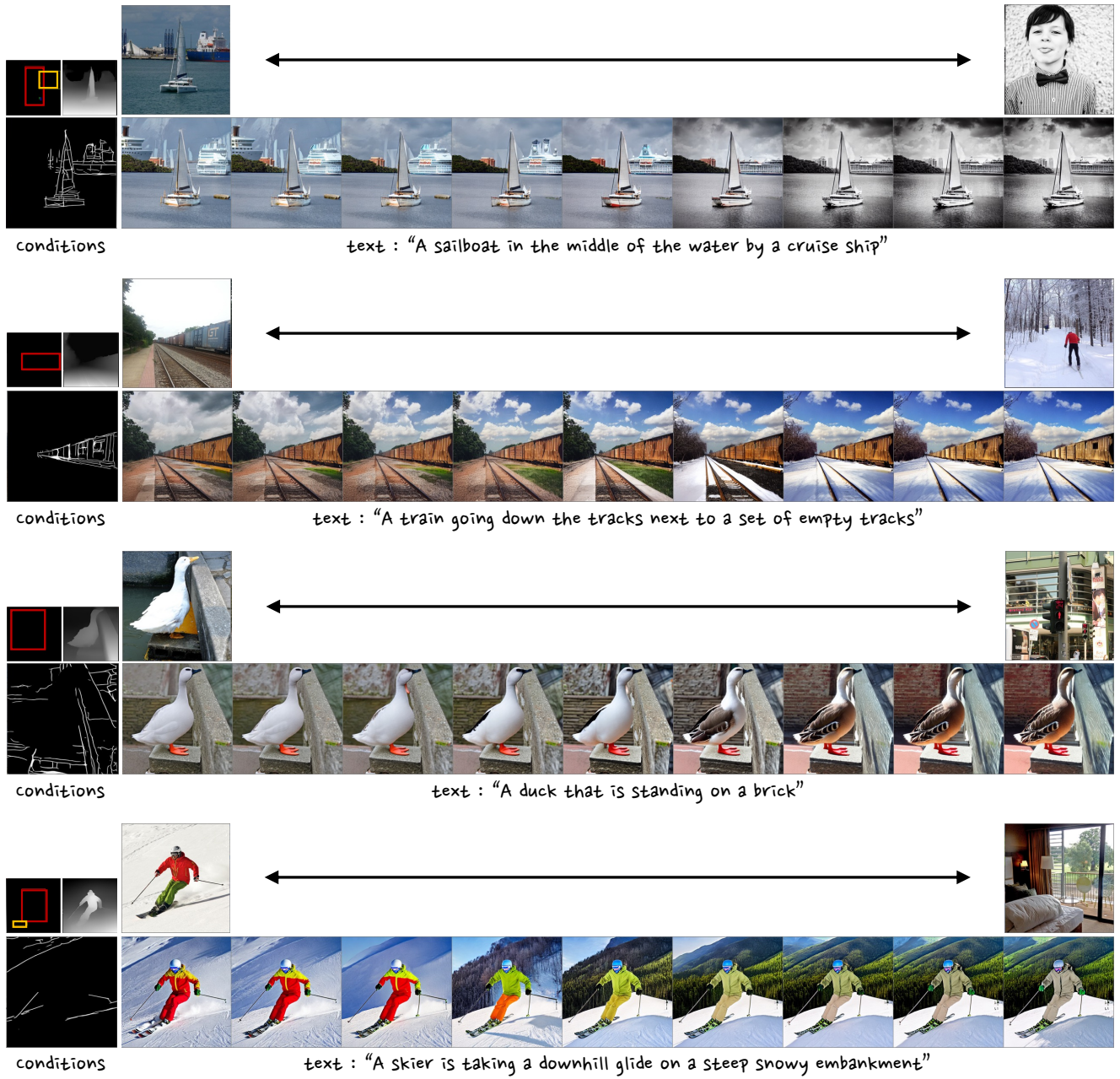
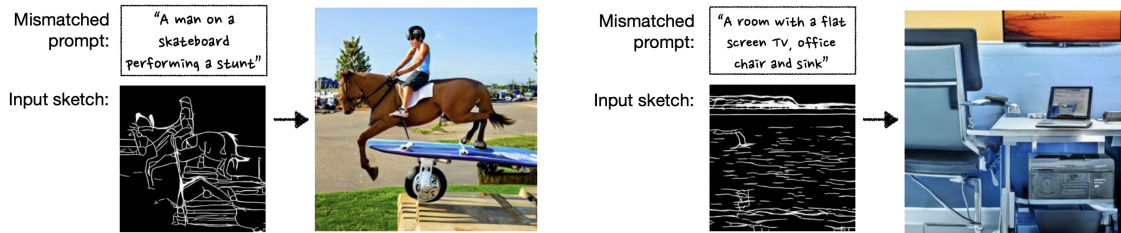


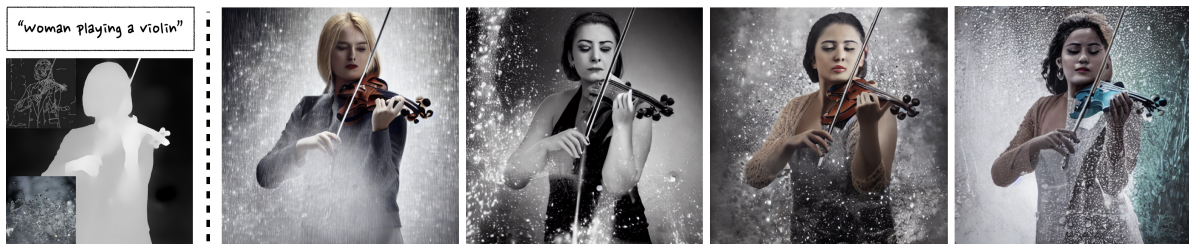
Figure 16. Interpolating latents for the style embedding.

D.5. Failure Cases

In this section, we examine instances where DIFFBLENDER encounters challenges in generating successful outputs. In Figure 17 (a), DIFFBLENDER exhibits incongruence as it processes multiple conditions simultaneously, attempting to preserve the input sketch while introducing novel objects or scenes that align with the provided text prompt. In cases where there is a mismatch between conditions, the quality of the output image is compromised as it attempts to incorporate all unmatched elements into a single image. In Figure 17 (b), DIFFBLENDER, being built upon SD [32], faces difficulties in overcoming the inherent limitations of SD, particularly in representing intricate elements. Noticeable artifacts are observed around the violinist's face and the violin bow, as well as unnatural hand depictions.



(a) Text prompt mismatching with the input sketch.



(b) Artifacts observed in human face and hands.

Figure 17. **Examples of failure cases.** (a) DIFFBLENDER processes multiple conditions concurrently, leading to instances where the provided conditions may not synergize seamlessly, such as text prompt mismatching with the input sketch. (b) Since DIFFBLENDER is constructed upon SD [32], it faces challenges in overcoming the inherent limitations of SD in representing intricate elements.